

Decentralized Poisson Multi-Bernoulli Filtering for Extended Target Tracking

Markus Fröhle, Karl Granström, Henk Wymeersch

Abstract—A decentralized Poisson multi-Bernoulli filter is proposed to track multiple extended targets using multiple sensors. Independent filters estimate the targets presence, state, and shape using a Gaussian process extent model; a decentralized filter is realized through fusion of the filters posterior densities. An efficient implementation is achieved by parametric state representation, utilization of single hypothesis tracks, and fusion of target information based on a fusion mapping. Numerical results demonstrate the performance.

Index Terms—Multitarget tracking, target extent, Gaussian processes, posterior fusion

I. INTRODUCTION

Multitarget tracking (MTT), i.e., tracking of independently moving targets, is important for surveillance and safety applications [1], [2]. Traditionally, it has been developed for surveillance of the sky using ground-to-air radar sensors. An MTT filter allows to incorporate the peculiarities of those kind of sensors: false alarm measurements due to clutter; missed detections; unknown measurement-to-target correspondence; and target appearance and disappearance; which are all challenges that arise for radar-like sensors. In many typical MTT scenarios, the sensor resolution is low with respect to (w.r.t.) the target size, and a reasonable assumption is to model the targets as points having a kinematic state (e.g., position and velocity).

With the availability of higher resolution sensors, the point target assumption does not hold anymore [3]. For instance, an autonomous driving car equipped with a high resolution Lidar sensor can obtain in one scan multiple detections from a single road user (e.g., car or cyclist), because the sensor resolution is high w.r.t. the target size. In such an application scenario, the target extent needs to be modeled (and estimated) as well in the MTT filter, leading to an extended target tracking (ETT) filter. In ETT, extended targets (ETs) give rise to possibly multiple noisy detections, the target shape is a priori unknown and may vary over time, and the objective is to estimate the ET's kinematic state as well the object shape [3].

A related objective may be found in computer vision, where multiple objects need to be estimated from single images or a sequence of images, with the difference that the camera provides a rich view of the environment. In contrast, in ETT

M. Fröhle, K. Granström, and H. Wymeersch are with the Department of Electrical Engineering, Chalmers University of Technology, Gothenburg, Sweden. E-mail: [>{frohle, karl.granstrom, henkw}@chalmers.se](mailto:{frohle, karl.granstrom, henkw}@chalmers.se). This work was supported, in part, by the EU-H2020 project HIGHTS (High Precision Positioning for Cooperative ITS Applications) under grant no. MG-3.5a-2014-636537 and COPPLAR (campus shuttle cooperative perception and planning platform) project, funded under grant no. 2015-04849 from Vinnova.

the ET's state and shape can seldom be estimated in a single time step due to the sparsity of the sensor measurements.

Different models for the ET shape exist in ETT, which may be classed according to complexity, ranging from not modeling the shape at all, to assuming a specific geometric shape with, e.g., unknown translation and rotation, to non-parametric models to describe, e.g., star convex object shapes. Typically, more complex models provide a richer shape description. Two popular models are the random matrix approach [4], where the target shape is described by an ellipsoid; and a non-parametric Gaussian process (GP) based approach [5], where a star convex target shape is described by a GP. Several ETT filters, have been developed, often extensions of their point target counterparts. Examples include: a particle filter for tracking a single ET [6], [7], and for tracking multiple ETs [8]–[11]. See [3] for an extensive overview of works on ETT.

Neither MTT nor ETT filters are bound to single sensors. Different approaches to incorporate measurements from multiple sensors which were acquired within one scan exist, where the simplest may be seen as performing multiple sequential Kalman update steps (or likewise) by augmenting the measurement model to incorporate all sensor models [12]. When sensors are geographically separated, measurements from all sensors need to be transmitted to the central processing unit where the filter is run. In the absence of such a unit, one can perform filtering already at the sensor and share only target track information, e.g., the parameters of a known probability density function (PDF) family. Through incorporation of target track information obtained by independent filters (i.e., information fusion), a decentralized filtering approach can be realized without the need for additional prior information. Such methods need to ensure that (unknown) common information obtained by the independent tracking filters is not double counted, e.g., the prior target density [13].

Depending on the type of posterior multiobject density in MTT/ETT filtering, several sub-optimal information fusion strategies have been developed based on, e.g, covariance intersection (CI) for Gaussian densities. This replaces the product form of Bayes' rule with the Kullback-Leibler average (KLA)¹. CI (and consequently KLA) is a method to fuse information with unknown priors in a robust way in the sense that the fused posterior is conservative and never overconfident about the estimates and thus implicitly sub-optimal [13], [14]. Examples include: fusion of Bernoulli and independent identically distributed (IID) cluster processes posteriors [15], fusion

¹In some literature this is known as exponential mixture density (EMD).

for Bernoulli filters [16], fusion for probability hypothesis density (PHD) and cardinalized PHD (CPHD) filters [17]–[22], and fusion for labeled multi-Bernoulli (LMB) filters [21], [23], [24].

In this paper, we utilize an ET shape model based on a GP and extend it to incorporate the known sensor state. We apply an ETT filter with this ET model, which allows tracking of multiple ETs. The resulting ETT filter's multiobject posterior is of Poisson multi-Bernoulli (PMB) form [25]. We propose a novel fusion strategy by separate fusion of undetected target densities in the form of Poisson point processs (PPPs), and detected target densities in the form of multi-Bernoulli (MB) random finite sets (RFSs); the latter is enabled by extending [23] to an arbitrary number of filters. The parametric implementation of the ETT filter yields a low complexity implementation locally, and globally through the introduction of a fusion map based on the Kullback-Leibler divergence (KLD) between target tracks. Simulation results demonstrate the performance of the proposed independent ETT filter as well as of the decentralized ETT filtering approach. Our main contributions of this paper are:

- We extend the GP model from [5], [8] for the ET shape to a multisensor scenario incorporating the sensors' state (position, orientation);
- We apply a state-of-the-art ETT filter (c.f. [26], [27]) using the extended GP based ET model and we propose a novel distributed fusion strategy based on the KLA by separate fusion of the PPPs and MB RFSs parts of the posterior multiobject density of PMB form; and
- We enable low complexity in distributed fusion through introduction of a fusion map based on KLD between target tracks.

The remainder of this paper is organized as follows; Section II gives some background knowledge on RFS, and Section III introduces the system model and the problem formulation. Section IV details the proposed ETT filter, Section V presents the decentralized posterior fusion approach using independent ETT filters, and Section VI addresses how the GP model for the ET shape is used in the ETT filter. Simulation results are given in Section VII, and conclusions are drawn in Section VIII.

II. BACKGROUND ON RFS

Two types of RFSs relevant for this work deserve special attention: Bernoulli RFS, and a PPP RFS. They can be extended to MB RFS, multi-Bernoulli mixture (MBM) RFS and combined in a Poisson multi-Bernoulli mixture (PMBM) RFS. These are described below, for more details on RFSs the reader is referred to [28].

Bernoulli RFS: A Bernoulli RFS \mathbf{X} has a multiobject density [28]

$$f(\mathbf{X}) = \begin{cases} 1 - r, & \mathbf{X} = \emptyset, \\ r f(\mathbf{x}), & \mathbf{X} = \{\mathbf{x}\}, \\ 0, & |\mathbf{X}| \geq 2, \end{cases} \quad (1)$$

where $r \in [0, 1]$ denotes the probability that a target exists and if it exists $f(\mathbf{x})$ is its PDF.

An MB RFS is the disjoint union of independent Bernoulli RFSs indexed by i . It is fully parametrized by $\{r_i, f_i(\mathbf{x})\}_{i \in \mathbb{I}}$, where \mathbb{I} is its index set. For $\mathbf{X} = \{\mathbf{x}_1, \dots, \mathbf{x}_n\}$, the multiobject density can be written as [23]

$$f(\mathbf{X}) = \sum_{\sigma} \sum_{I \in \mathcal{F}_n(\mathbb{I})} \prod_{i=1}^n r_{I_n(i)} f_{I_n(i)}(\mathbf{x}_{\sigma(i)}) \prod_{k=1}^{|I^C|} (1 - r_{I_n^C(k)}), \quad (2)$$

where $\mathcal{F}_n(\mathbb{I})$ is the space of all finite subsets of length n of the index set \mathbb{I} , $I^C = \mathbb{I} \setminus I$ is the complement set, and I_n and I_n^C are ordered vectors of the sets I and I^C , respectively. An alternative form to express $f(\mathbf{X})$ is

$$f(\mathbf{X}) = \sum_{\mathbf{u}_i \in \mathbf{X}_i = \mathbf{X}} \prod_{i \in \mathbb{I}} f_i(\mathbf{X}_i) \quad (3)$$

for $|\mathbf{X}| \leq |\mathbb{I}|$, and $f(\mathbf{X}) = 0$ otherwise. The multiobject density of an MBM is the normalized, weighted sum of multiobject densities of MBs, which can be stated as [26]

$$f(\mathbf{X}) = \sum_{j \in \mathbb{J}} w_j \sum_{\mathbf{u}_i \in \mathbf{X}_i = \mathbf{X}} \prod_{i \in \mathbb{I}^j} f_{j,i}(\mathbf{X}_i). \quad (4)$$

The MBM multiobject density is parametrized by $\{w_j, \{r_{j,i}, f_{j,i}(\mathbf{x})\}_{i \in \mathbb{I}^j}\}_{j \in \mathbb{J}}$, where w_j is the weight of MB j , and \mathbb{J} is the index set of the MBs in the MBM. The notation, $\mathbf{X}_1 \uplus \mathbf{X}_2 = \mathbf{X}$ means $\mathbf{X}_1 \cup \mathbf{X}_2 = \mathbf{X}$ and $\mathbf{X}_1 \cap \mathbf{X}_2 = \emptyset$. An MB is therefore a special case of an MBM with $|\mathbb{J}| = 1$.

PPP RFS: A PPP is a type of RFS, where the cardinality follows a Poisson distribution, and its elements are IID. It is parametrized by the intensity function $D(\mathbf{x}) = \lambda f(\mathbf{x})$, where $\lambda > 0$ is the Poisson rate and $f(\mathbf{x})$ is a PDF on the single element state \mathbf{x} . The multiobject density of a PPP is [26], [28]

$$f(\mathbf{X}) = e^{-\lambda} \prod_{i=1}^n \lambda f(\mathbf{x}_i). \quad (5)$$

PMBM RFS: A PMBM RFS is created by disjoint set union of an PPP and an MBM having multiobject density [26]

$$f(\mathbf{X}) = \sum_{\mathbf{X}^u \uplus \mathbf{X}^d = \mathbf{X}} f^u(\mathbf{X}^u) f^d(\mathbf{X}^d), \quad (6)$$

where $f^u(\cdot)$ has multiobject density (5), and $f^d(\mathbf{X}^d)$ has multiobject density (4). For $|\mathbb{J}| = 1$, (6) is called a PMB distribution.

A. RFS Bayesian Filter

Similar to the random vector (RV) case, an RFS based filter can be described, conceptually at least, within the Bayesian filtering framework by performing a prediction step using the motion model [2, Ch. 14]

$$f_+(\mathbf{X}) = \int f(\mathbf{X}|\mathbf{X}') f_-(\mathbf{X}') \delta \mathbf{X}', \quad (7)$$

where $f_-(\mathbf{X}')$ is the prior RFS density, $f(\mathbf{X}|\mathbf{X}')$ is the multiobject process model, and a Bayesian update step

$$f(\mathbf{X}|\mathbf{Z}) \propto \ell(\mathbf{Z}|\mathbf{X}) f_+(\mathbf{X}). \quad (8)$$

Here, $f_+(\mathbf{X})$ is the predicted RFS density, and $\ell(\mathbf{Z}|\mathbf{X})$ is the RFS measurement likelihood for measurement set \mathbf{Z} .

B. Multiobject estimation

A typical way to estimate the set states from a Bernoulli process with RFS density $f(\mathbf{X})$ is by comparing the probability of existence r to an existence threshold r_{th} . For $r > r_{\text{th}}$, the state (target) is said to exist and has PDF $f(\mathbf{x})$. Its state can then be estimated by the mean $\hat{\mathbf{x}} = \int \mathbf{x} f(\mathbf{x}) d\mathbf{x}$. See, e.g., [29] for a longer discussion on multiobject estimation.

III. SYSTEM MODEL AND PROBLEM FORMULATION

Here, we present first the state and motion model of a single ET. This is followed by measurement model, and the problem formulation.

A. ET state and motion model

The augmented state $\mathbf{x}_k = [\gamma_k, \mathbf{y}_k^T]^T$ of a single ET at time k comprises an unknown Poisson rate γ_k of number of measurements generated by the ET and the ET spatial state \mathbf{y}_k (which will be detailed later). The state has prior PDF

$$f(\mathbf{x}_k) = \mathcal{G}(\gamma_k; \alpha_k, \beta_k) \mathcal{N}(\mathbf{y}_k; \hat{\mathbf{y}}_k, \mathbf{P}_k), \quad (9)$$

where the gamma distribution with parameters α_k and β_k is a conjugate prior for the rate γ_k , and the Gaussian distribution with mean $\hat{\mathbf{y}}_k$ and covariance matrix \mathbf{P}_k describes the a priori knowledge regarding the ET spatial state \mathbf{y}_k .

A standard motion model for the ET is assumed, where ET motion follows IID Markov processes with single ET transition PDF $f_{k+1|k}(\mathbf{x}_{k+1}|\mathbf{x}_k)$. Targets arrive according to a non-homogeneous PPP with intensity $D^b(\mathbf{x})$, and depart according to IID Markov processes, where the survival probability in \mathbf{x}_k is $p_S(\mathbf{x}_k)$.

Remark 1: Note that in the augmented state PDF (9) the measurement rate γ_k and the ET state (including its extent) \mathbf{y}_k are considered independent, which is a common assumption in ETT (see e.g. [30]). Due to the sensor-to-target geometry (e.g., for a Lidar its angular resolution and the sensor-target distance), the estimated measurement rate of the ET is implicitly sensor dependent, i.e., a different sensor configuration yields a different estimate for γ_k . The explicit modeling of the dependence of γ_k on the sensor state and \mathbf{y}_k is not considered here.

B. ET measurement model

In this section, the time index k will be omitted for the sake of brevity. In one scan, a sensor receives a set of measurements \mathbf{Z} consisting of target-generated measurements and clutter, where the ETs are independently detected with state-dependent probability of detection $p_D(\mathbf{x})$. Clutter is modeled by a PPP with intensity $\kappa(\mathbf{z}) = \lambda c(\mathbf{z})$ with mean λ and spatial distribution $c(\mathbf{z})$. Target-generated measurements are modeled by a PPP with intensity $\gamma(\mathbf{x})f(\mathbf{z}|\mathbf{x})$, where both the Poisson measurement rate $\gamma(\mathbf{x})$ and the single measurement likelihood $f(\mathbf{z}|\mathbf{x})$ are state dependent. The measurement likelihood for ETs $\{\mathbf{x}_1, \dots, \mathbf{x}_n\}$ and measurement set \mathbf{Z} is

$$\ell(\mathbf{Z}|\{\mathbf{x}_1, \dots, \mathbf{x}_n\}) = e^{-\lambda} \sum_{\mathbf{Z}_c \cup \mathbf{Z}_1 \cup \dots \cup \mathbf{Z}_n = \mathbf{Z}} [c(\cdot)]^{\mathbf{Z}_c} \prod_{i=1}^n \ell_{\mathbf{Z}_i}(\mathbf{x}_i), \quad (10)$$

where $[c(\cdot)]^{\mathbf{Z}_c}$ is shorthand for $\prod_{\mathbf{z} \in \mathbf{Z}_c} c(\mathbf{z})$, $[c(\cdot)]^\emptyset = 1$ by definition, and [26]

$$\ell_{\mathbf{Z}}(\mathbf{x}) = \begin{cases} p_D(\mathbf{x})e^{-\gamma(\mathbf{x})} \prod_{\mathbf{z} \in \mathbf{Z}} \gamma(\mathbf{x})f(\mathbf{z}|\mathbf{x}), & |\mathbf{Z}| > 0, \\ (1 - p_D(\mathbf{x})) + p_D(\mathbf{x})e^{-\gamma(\mathbf{x})}, & \mathbf{Z} = \emptyset. \end{cases} \quad (11)$$

Note that (10) involves potentially multiple ETs, leading to a data association (DA) problem.

C. Problem Formulation

We consider a scenario with N_{sens} sensing systems (each composed of sensors plus filter), each collecting measurements using its local sensors. Our goals are (i) to derive a low-complexity PMB-ETT filter for each sensing system $s = 1, 2, \dots, N_{\text{sens}}$, computing in every time step k the posterior density $f_s(\mathbf{X}_k|\mathbf{Z}_{s,k:1})$ of the ETs, using only its own sensors with measurement set $\mathbf{Z}_{s,k:1}$; and (ii) to derive a decentralized method to combine posterior information of ETs obtained by N_{sens} independent ETT filters in order to obtain a global posterior density $\bar{f}_w(\mathbf{X}_k|\mathbf{Z}_{1,k:1}, \mathbf{Z}_{2,k:1}, \dots, \mathbf{Z}_{N_{\text{sens}},k:1})$ (i.e., using only the *posterior* densities of each ETT filter).

IV. INDEPENDENT ET-PMB FILTER

In this section, we describe the processing performed by each PMB-ETT filter from [26]. We again omit the time index k for clarity. The PMB model is a combination of a PPP describing the distribution of unknown targets, i.e., targets which are hypothesized to exist, but have not yet been detected; and a MB which describes targets that have been detected at least once. The target set can therefore be split into two disjoint subsets $\mathbf{X} = \mathbf{X}^u \uplus \mathbf{X}^d$ corresponding to the unknown target set \mathbf{X}^u (with intensity $D^u(\mathbf{x})$) and the detected target set \mathbf{X}^d with density $f^d(\mathbf{X}^d)$ and index set \mathbb{I} . Hence, the PMB density is fully described by a MB component: $\{r^i, f^i(\mathbf{x})\}_{i \in \mathbb{I}}$ and a PPP component $D^u(\mathbf{x})$.

A. ET-PMB Filter Prediction

The predicted density is a PMB density with parameters [26, Sec. IV], [27]

$$D_+^u = D^b(\mathbf{x}) + \langle D^u, p_S f_{k+1|k} \rangle, \quad (12)$$

$$r_+^i = \langle f^i, p_S \rangle r^i, \quad (13)$$

$$f_+^i = \frac{\langle f^i, p_S f_{k+1|k} \rangle}{\langle f^i, p_S \rangle}, \quad (14)$$

where $\langle g, h \rangle = \int g(\mathbf{x})f(\mathbf{x})d\mathbf{x}$ denotes the inner product. The proof of the prediction step can be found in, e.g., [25].

B. ET-PMB filter update

We introduce the set of valid DAs $\mathcal{A} = \mathcal{P}(\mathbb{M} \cup \mathbb{I})$, where \mathbb{M} is the index set for \mathbf{Z} , where $A \in \mathcal{A}$ is a partition of $\mathbb{M} \cup \mathbb{I}$ into non-empty disjoint subsets $C \in A$ (called index cells), with the constraint that for each $C : |C \cap \mathbb{I}| \leq 1$ (i.e., measurements can only be associated with a single target). When $|C \cap \mathbb{I}| = 1$, let the entry in $C \cap \mathbb{I}$ be denoted by i_C and let $C_C = \cup_{m \in C \cap \mathbb{M}} \mathbf{z}_m$ contain the associated measurements.

Given the predicted prior PMB density with parameters (12), (13), (14), and a set of measurements \mathbf{Z} ; the updated density is a PMBM density [26, Sec. IV], [27]

$$f(\mathbf{X}|\mathbf{Z}) = \sum_{\mathbf{X}^u \uplus \mathbf{X}^d = \mathbf{X}} f^u(\mathbf{X}^u) \sum_{A \in \mathcal{A}} w_A f_A^d(\mathbf{X}^d), \quad (15)$$

$$f^u(\mathbf{X}^u) = e^{-\langle D^u, 1 \rangle} \prod_{\mathbf{x} \in \mathbf{X}^u} D^u(\mathbf{x}), \quad (16)$$

$$f_A^d(\mathbf{X}^d) = \sum_{\mathbf{C} \in \mathcal{A}} \prod_{C \in A} f_C(\mathbf{X}^C), \quad (17)$$

$$D^u(\mathbf{x}) = q_D(\mathbf{x}) D_+^u(\mathbf{x}), \quad (18)$$

where $f_C(\mathbf{X}^C)$ is a Bernoulli density, with existence probability and spatial distribution provided in Appendix A, together with the weights w_A of each DA hypothesis. Above, $q_D(\mathbf{x})$ denotes the probability that the target \mathbf{x} is not detected and is defined as

$$q_D(\mathbf{x}) = 1 - p_D(\mathbf{x}) + p_D(\mathbf{x}) e^{-\gamma(\mathbf{x})}. \quad (19)$$

Remark 2: The number of possible partitions of the measurement set \mathbf{Z} is given by the Bell number of order equal to the number of measurements [26]. To reduce computational complexity, we use standard methods and truncate the space of possible partitions by clustering measurements and consider DA w.r.t. different clusters. Note that it has been shown in literature that clustering can be applied as a pre-processing step without distorting filtering performance (see, e.g., [31]–[33]).

C. Conversion to PMB Density

Due to the sum over DA hypotheses in (15), the posterior multiobject density is a PMBM. To bring it into the PMB form of the prior, which is also the form used for the posterior fusion proposed in Section V, several approaches are possible, including approximating the posterior PMBM by a PMB in the minimum KLD sense as proposed in [34] for point targets and in [35] for ETs. Here, will consider a low-complexity suboptimal approach by replacing the sum over DAs by the max operator over the DA hypothesis weights w_A , i.e., approximating the PMBM posterior by a PMB which consists of the MB in the MBM that has highest weight.

D. Extension to Multi-sensor Setup

In a multisensor setup, i.e., where a single filter receives (possibly multiple) measurements from multiple sensors, a measurement set \mathbf{Z}_s is obtained from each sensor $s \in 1, 2, \dots, N_{\text{sens}}$. The posterior PMBM density incorporating all measurements from all sensors is denoted $f(\mathbf{X}|\mathbf{Z}_{1:N_{\text{sens}}})$, where measurements from all sensors are consolidated. This leads to a rapid increase of the DA space \mathcal{A} with increasing N_{sens} . To enable a tractable implementation of the ET-PMB filter, one can apply an iterator-corrector approach, where measurement sets from multiple sensors are incorporated in a sequential manner by using the posterior density obtained after updating by measurements collected by one sensor as the prior density for the update step with measurements collected by the next sensor. In doing so, all measurements from all

sensors need to be sent to a central processing unit where the filter is run. This can be difficult for geographically separated sensors, which communicate, e.g., over the wireless channel.

Instead, with a processing unit at each sensor (and hence an independent filter) only compressed information, in terms of the parameters of the posterior densities, need to be transmitted between the units. Through combination of the posterior densities $f_s(\mathbf{X}|\mathbf{Z}_s)$ of each individual filter $s \in 1, 2, \dots, N_{\text{sens}}$ (with measurements from sensor s) the global posterior $f(\mathbf{X}|\mathbf{Z}_{1:N_{\text{sens}}})$ can be obtained, which is described in the next section.

V. DECENTRALIZED POSTERIOR FUSION

Here, we present a decentralized approach to robust fusion of posterior densities $f_s(\mathbf{X}|\mathbf{Z}_s)$ computed by independent ETT filters with unknown prior densities. Since we considered the measurement rate to be independent of the sensor state (c.f. (9)), fusion is only applied to the spatial state \mathbf{y} , while each sensor maintains a local density of the rate of each target. We indicate this by writing the posteriors as $f_s(\mathbf{Y}|\mathbf{Z}_s)$ for all s .

A. Robust Posterior Fusion: Principle

Robust posterior fusion can be achieved by minimizing the KLA between RFS densities $f(\cdot)$ and $f_s(\cdot)$ for $s = 1, \dots, N_{\text{sens}}$ with respect to $f(\cdot)$. The KLA is defined as [20]

$$\bar{f}_\omega = \arg \inf_f \sum_{s=1}^{N_{\text{sens}}} \omega_s D(f\|f_s), \quad (20)$$

for any combinations of weights $\omega_s \in [0, 1] : \sum_s \omega_s = 1$. We have introduced $D(f\|f_s)$ as the KLD between RFS densities $f(\mathbf{Y}|\mathbf{Z}_{1:N_{\text{sens}}})$ and $f_s(\mathbf{Y}|\mathbf{Z}_s)$ defined as [20]

$$D(f\|f_s) = \int f(\mathbf{Y}|\mathbf{Z}_{1:N_{\text{sens}}}) \log \frac{f(\mathbf{Y}|\mathbf{Z}_{1:N_{\text{sens}}})}{f_s(\mathbf{Y}|\mathbf{Z}_s)} \delta \mathbf{Y}. \quad (21)$$

The fused posterior (20) is robust in the sense that the fused posterior is conservative and is never overconfident w.r.t. the true target uncertainty [13]. The problem (20) was shown to have a closed-form solution [20]

$$\bar{f}_\omega(\mathbf{Y}|\mathbf{Z}_{1:N_{\text{sens}}}) = \frac{\prod_{s=1}^{N_{\text{sens}}} f_s(\mathbf{Y}|\mathbf{Z}_s)^{\omega_s}}{\int \prod_{s'=1}^{N_{\text{sens}}} f_{s'}(\mathbf{Y}|\mathbf{Z}_{s'})^{\omega_{s'}} \delta \mathbf{Y}}. \quad (22)$$

Note that (22) is a generalization of the Uhlmann-Julier covariance intersection method (c.f. [13]) for posterior RFSs densities with unknown priors [14].

Remark 3: The weights ω_s can be chosen such that (22) is as peaky as possible. According to [14], this is achieved when the following supremal value is maximized

$$\max_{\{\omega_s\}_{s=1}^{N_{\text{sens}}}} \sup_{\mathbf{Y}} \frac{\kappa^{|\mathbf{Y}|}}{|\mathbf{Y}|!} \bar{f}_\omega(\mathbf{Y}|\mathbf{Z}_{1:N_{\text{sens}}}) \quad (23)$$

$$\text{s.t. } \omega_s \geq 0, \forall s \quad (24)$$

$$\sum_{s=1}^{N_{\text{sens}}} \omega_s = 1, \quad (25)$$

where κ is a constant with units such that the objective is unitless. Alternatively, for $f_s(\mathbf{Y}|\mathbf{Z}_s)$ a MB with components

$\{r^i, f^i(\mathbf{y})\}_{i \in \mathbb{I}}$ and where each Bernoulli component has a Gaussian PDF $f^i(\mathbf{y}) = \mathcal{N}(\mathbf{y}; \mu_i, P_i)$ for all i with mean vector μ_i and covariance matrix P_i , a suboptimal adaptive approach to determine the fusion weights ω_s can be found by maximizing the minimum information over all ETs. In doing so, we extract all existing Bernoulli components from $f_s(\mathbf{Y}|\mathbf{Z}_s)$ for $s = 1, \dots, N_{\text{sens}}$. Next, we identify Bernoulli components which are representing the same ET. In doing so, we first extract the ETs state (c.f. Sec. II-B) and then solve, e.g., a linear assignment problem with KLD as cost between the ET's PDF. This procedure will be explained in Sec. V-C. We then define the Fisher information matrix (FIM) per ET as

$$J_n = \sum_{s=1}^{N_{\text{sens}}} \omega_s P_{n,s}^{-1}, \quad (26)$$

where $n = 1, \dots, N$ enumerates the ETs, and $P_{n,s}$ is the covariance matrix for the n -th ET extracted from the MB of filter s . The fusion weights ω_s maximizing the minimum information over all ETs are then found by the solution of the linear program

$$\max_{\{\omega_s\}_{s=1}^{N_{\text{sens}}}} \min_n \text{tr}(J_n) \quad (27)$$

$$\text{s.t. } \omega_s \geq 0, \forall s \quad (28)$$

$$\sum_{s=1}^{N_{\text{sens}}} \omega_s = 1 \quad (29)$$

where $\text{tr}(J_n)$ denotes the trace of matrix J_n . The FIM J_n captures the amount of fused information we have about target n . Therefore, by finding weights that maximise the minimal FIM, we ensure that the FIM for each target is at least as good as the target function (27).

B. Robust PMB Posterior Fusion

Since the posterior density of each ETT filter is a PMB and to utilize the fused posterior density as prior for the next time step in the ETT filter, it should be of the PMB form, i.e.,

$$\bar{f}_\omega(\mathbf{Y}|\mathbf{Z}_{1:N_{\text{sens}}}) = \sum_{\mathbf{Y}^u \oplus \mathbf{Y}^d = \mathbf{Y}} \bar{f}_\omega^u(\mathbf{Y}^u|\mathbf{Z}_{1:N_{\text{sens}}}) \times \bar{f}_\omega^d(\mathbf{Y}^d|\mathbf{Z}_{1:N_{\text{sens}}}) \quad (30)$$

comprised of a PPP $\bar{f}_\omega^u(\mathbf{Y}^u|\mathbf{Z}_{1:N_{\text{sens}}})$ modeling the unknown targets and a MB $\bar{f}_\omega^d(\mathbf{Y}^d|\mathbf{Z}_{1:N_{\text{sens}}})$ modeling detected targets. Therefore, it becomes natural to consider unknown targets separately from detected targets. This motivates the use of the following bound on the KLD [36, Thm. I]

$$D(\bar{f}_\omega \| f_s) \leq D(\bar{f}_\omega^u \| f_s^u) + D(\bar{f}_\omega^d \| f_s^d). \quad (31)$$

In this case, the PMB attaining the KLA is found by separately solving (20) for the PPP resulting in $\bar{f}_\omega^u(\mathbf{Y}|\mathbf{Z}_{1:N_{\text{sens}}})$, and for the MB resulting in $\bar{f}_\omega^d(\mathbf{Y}|\mathbf{Z}_{1:N_{\text{sens}}})$. We now proceed with the calculation of the KLA for the PPP and MB RFSs separately, allowing to find the fused posterior $\bar{f}_\omega(\mathbf{Y}|\mathbf{Z}_{1:N_{\text{sens}}})$. In what follows, the posterior of each ETT filter posterior $f_s(\mathbf{Y}|\mathbf{Z}_s)$ is of PMB form for $s = 1, \dots, N_{\text{sens}}$.

1) *Fusion of PPP RFSs:* The PPP RFS with multiobject density $f_s^u(\mathbf{Y}|\mathbf{Z}_s)$ has intensity $D_s^u(\mathbf{y}) = \lambda_s f_s(\mathbf{y})$. Then the fused posterior of the PPPs minimizing the KLA (c.f. (20)) for given weights ω_s has PHD [15]

$$\bar{D}^u(\mathbf{y}) = \bar{\lambda} \bar{f}(\mathbf{y}), \quad (32)$$

where the expected number of targets and target density are

$$\bar{\lambda} = \prod_{s=1}^{N_{\text{sens}}} \mu_s^{\omega_s} \int \prod_{s'=1}^{N_{\text{sens}}} f_{s'}(\mathbf{y})^{\omega_{s'}} d\mathbf{y} \quad (33)$$

and

$$\bar{f}(\mathbf{y}) = \frac{\prod_{s=1}^{N_{\text{sens}}} f_s(\mathbf{y})^{\omega_s}}{\int \prod_{s'=1}^{N_{\text{sens}}} f_{s'}(\mathbf{y})^{\omega_{s'}} d\mathbf{y}}, \quad (34)$$

respectively.

Remark 4: The above integrals are in general not tractable, however, closed-form expressions are possible in some cases. We illustrate this when $f_s(\mathbf{y}) = \mathcal{N}(\mathbf{y}; \mu_s, P_s)$ is Gaussian with parameters μ_s and P_s . In that case, [20, Eqn. 36]

$$\mathcal{N}(\mathbf{y}; \mu, P)^\omega = \frac{\det(2\pi P \omega^{-1})^{\frac{1}{2}}}{\det(2\pi P)^{\frac{\omega}{2}}} \mathcal{N}(\mathbf{y}; \mu, P \omega^{-1}) \quad (35)$$

and the products of such terms can be easily computed with the help of the formulas from [37]. For the case of $N_{\text{sens}} = 2$ sensors, $f_1(\mathbf{y}_1)^{\omega_1} f_2(\mathbf{y}_2)^{\omega_2} = \xi \mathcal{N}(\mathbf{y}; \bar{\mu}, \bar{P})$, where

$$\xi = \frac{\det(2\pi P_1 \omega_1^{-1})^{1/2}}{\det(2\pi P_1)^{\omega_1/2}} \frac{\det(2\pi P_2 \omega_2^{-1})^{1/2}}{\det(2\pi P_2)^{\omega_2/2}} \times \mathcal{N}(\mu_1 - \mu_2; 0, P_1 \omega_1^{-1} + P_2 \omega_2^{-1}), \quad (36)$$

$$\bar{P} = (\omega_1 P_1^{-1} + \omega_2 P_2^{-1})^{-1}, \quad (37)$$

$$\bar{\mu} = \bar{P}(\omega_1 P_1^{-1} \mu_1 + \omega_2 P_2^{-1} \mu_2). \quad (38)$$

Hence, the integral in (33)–(34) evaluates to ξ , and the expected number of targets (33) becomes $\bar{\lambda} = \xi \lambda_1^{\omega_1} \lambda_2^{\omega_2}$.

2) *Fusion of MB RFSs:* Here, we discuss fusion of the MB part of the PMB posterior multiobject densities. We first note that calculating (22) involves the partial fraction power of a MB multiobject density. In doing so, we utilize the result of [20], [23], [24] that for well separated targets, i.e., when $|\int \mathbf{y} f_{s,i}(\mathbf{y}) d\mathbf{y} - \int \mathbf{y} f_{s,j}(\mathbf{y}) d\mathbf{y}|$ is large for any $i, j \in \mathbb{I}_s$, we can approximate [23]

$$f_s^d(\{\mathbf{y}_1, \dots, \mathbf{y}_n\}|\mathbf{Z}_i)^{\omega_s} \approx \sum_{\sigma} \sum_{I \in \mathcal{F}_n(\mathbb{I})} \prod_{i=1}^n r_{I(i)}^{\omega_s} f_{I(i)}(\mathbf{y}_{\sigma(i)})^{\omega_s} \times \prod_{k \in I^C(I)} (1 - r_k)^{\omega_s}, \quad (39)$$

in which we recall that I^C is induced by I . We distinguish two cases: (i) where all the sensors have the same field-of-view (FoV); (ii) where sensors may have a different FoV. We assume that for each sensor the pose is known, and it then follows that the FoV is known. This can be the case for sensors mounted on a fixed known location, as well as for sensors mounted on a moving platform, if their location and pose is estimated using, e.g., a global navigation satellite system (GNSS) receiver in connection with an inertial measurement unit (IMU).

Same FoV: We order the sensors according to ascending number of detected targets, i.e., such that $|\mathbb{I}_1| \leq |\mathbb{I}_2| \dots \leq |\mathbb{I}_{N_{\text{sens}}}|$. We then define a *fusion map* [23], [38] $\theta : \mathbb{I}_1 \rightarrow \mathbb{I}_2 \times \mathbb{I}_3 \dots \times \mathbb{I}_{N_{\text{sens}}}$, such that $\theta(i) = \theta(i')$ implies $i = i'$. The space of all fusion maps induced by the set $I \in \mathcal{F}(\mathbb{I}_1)$ of an agent with index set \mathbb{I}_1 is called fusion map space denoted Θ_{I_1} . Hence, $\theta(I_1(i))$ is a vector of length $N_{\text{sens}} - 1$, where the $s - 1$ -th element is the MB component of the s -th sensor that is mapped from $I_1(i)$ -th component of the first sensor. With a slight abuse of notation, we introduce $I_s^C(\theta(I_1))$ as the complement of \mathbb{I}_s with respect to the mapping of \mathbb{I}_1 to \mathbb{I}_s , i.e., the elements in \mathbb{I}_s that were not mapped to an element in \mathbb{I}_1 . Under the approximation (39), we extend [23] to allow a fusion with N_{sens} MBs so that the numerator of (22) becomes (40)–(43) (illustrated on top of the next page), where

$$\begin{aligned} \tilde{w}_{I_1, \theta} &= \prod_{i=1}^n Z_{I_1(i), \theta(I_1(i))} r_{1, I_1(i)}^{\omega_1} \prod_{s>1} r_{s, [\theta(I_1(i))]_{s-1}}^{\omega_s} \\ &\times \prod_{k \in I_1^C(I_1)} (1 - r_{1, k})^{\omega_1} \prod_{k' \in I_s^C(\theta(I_1))} (1 - r_{s, k'})^{\omega_s}, \end{aligned} \quad (44)$$

$$Z_{i, \theta(i)} = \int f_{1, i}(\mathbf{y})^{\omega_1} \prod_{s>1} f_{s, \theta(i)}(\mathbf{y})^{\omega_s} d\mathbf{y}, \quad (45)$$

$$f_{\omega, i, \theta(i)} = \frac{f_{1, i}(\mathbf{y})^{\omega_1} \prod_{s>1} f_{s, [\theta(i)]_{s-1}}(\mathbf{y})^{\omega_s}}{Z_{i, \theta(i)}}. \quad (46)$$

The fused posterior of detected targets is, according to (22),

$$\bar{f}_{\omega}^d(\mathbf{Y} | \mathbf{Z}_{1:N_{\text{sens}}}) = \frac{\prod_s f_s^d(\mathbf{Y} | \mathbf{Z}_s)^{\omega_s}}{W}, \quad (47)$$

where the numerator under approximation (39) is (43) and the denominator is

$$W = \sum_{I_1 \in \mathcal{F}(\mathbb{I}_1)} \sum_{\theta \in \Theta_{I_1}} \tilde{w}_{I_1, \theta}. \quad (48)$$

Note that the first sum goes over all finite subsets of \mathbb{I}_1 .

Different FoV: When the FoVs of the sensors are not equal, the above procedure can still be applied to pairs of sensors with targets that are in the intersection of the FoVs. This procedure is then carried out sequentially between each pair of sensors. MB components outside the intersection of the FoV are not fused.

3) *Conversion to a PMB Density:* Fusing MBs by calculation of (47) does not result in an MB. Using first-order moment matching, the MB that approximates (47) can be recovered [23, Sec. III-C] with parameters

$$\{r_{\omega, i}^d, f_{\omega, i}^d\}_{i \in \mathbb{I}_1}, \quad (49)$$

where

$$r_{\omega, i}^d = \sum_{I_1 \in \mathcal{F}(\mathbb{I}_1)} \sum_{\theta \in \Theta_{I_1}} 1_{I_1}(i) w_{I_1, \theta}, \quad (50)$$

$$f_{\omega, i}^d = \frac{1}{r_{\omega, i}^d} \sum_{I_1 \in \mathcal{F}(\mathbb{I}_1)} \sum_{\theta \in \Theta_{I_1}} 1_{I_1}(i) w_{I_1, \theta} f_{\omega, i, \theta(i)}, \quad (51)$$

where $w_{I_1, \theta} = \tilde{w}_{I_1, \theta}/W$ and operator $1_I(i) = 1$ for $i \in I$ and zero otherwise. In order to calculate (50) and (51), we need to consider all possible fusion mappings $\theta \in \Theta_{I_1}$ for finite subset $I_1 \in \mathcal{F}(\mathbb{I}_1)$.

4) Overall procedure: In order to apply the fusion of PMB posteriors obtained by ETT filters, as described in Section V-B, we apply the fusion of PPPs and MBs separately allowing to find the KLA (c.f. (20) and (31)). Since the ETT filter prior is of form PMB, the fused posterior, which is also a PMB, can be used without modification in the filter. It can then be used as prior density in the next time step. Furthermore, posterior fusion can be performed after every update step of the ETT filters or based on a lower rate depending on the application and communication capabilities.

C. Complexity Reduction

Since we already assume targets are well separated in space, which enabled (39), in general it holds that only one $\tilde{w}_{I_1, \theta}$ of all $\theta \in \Theta_{I_1}$ in (50) (and (51)) will have significantly non-zero weight. Therefore, we propose to replace the summation over θ by usage of the fusion mapping maximizing this sum term denoted the *best fusion map* θ^* . In this case, Bernoulli components $j \in \mathbb{I}_s$ not part of the best fusion map θ^* do not contribute in the calculation of (50) and (51). Therefore, we propose to use recycling (c.f. [36]) of those Bernoulli components before the PPP and MB fusion is done. Note, recycling approximates a Bernoulli component (of the MB) by an independent PPP allowing to incorporate it in the PPP RFS of the PMB. The quality of this approximation is best for low values of probability of existence [36].

The best fusion map can be found as follows. Let there be two PMBs with index sets \mathbb{I}_1 and \mathbb{I}_s respectively. We define the best fusion map $\theta^* \in \Theta_{I_1}$ as the solution of the optimal assignment problem [39]

$$\begin{aligned} \underset{L}{\text{minimize}} \quad & \sum_{n=1}^{|\mathbb{I}_1|} \sum_{m=1}^{|\mathbb{I}_s|} L_{n, m} V_{n, m} \\ \text{subject to} \quad & \sum_{m=1}^{|\mathbb{I}_s|} L_{n, m} = 1, \forall n, \\ & L_{n, m} \in \{0, 1\}, \end{aligned} \quad (52)$$

where $V_{n, m}$ denotes the cost for assigning (mapping) Bernoulli n in MB 1 with Bernoulli m in MB s . To solve (52), we can use, e.g., the Munkres algorithm [40], [41]. For $N_{\text{sens}} > 2$ the best fusion map is found by sequentially solving (52) for $s = 2, \dots, N_{\text{sens}}$.

We define the cost metric in terms of the KLD between the PDFs of the Bernoulli components in MB 1 and s . For a Bernoulli component $n \in \mathbb{I}_1$ with parameters $r_{1, n}$ and $f_{1, n}(\mathbf{y})$ of form (9), and similarly for $m \in \mathbb{I}_s$, the cost is defined

$$V_{n, m} = \frac{1}{2} [D(f_{1, n} \| f_{s, m}) + D(f_{s, m} \| f_{1, n})], \quad (53)$$

where for Gaussian PDFs $f_{1, n}(\mathbf{y}) = \mathcal{N}_0(\mathbf{y}; \mu_0, \Sigma_0)$ and $f_{s, m}(\mathbf{y}) = \mathcal{N}_1(\mathbf{y}; \mu_1, \Sigma_1)$ of RV \mathbf{y} with dimension k , the KLD has closed form solution

$$\begin{aligned} D(f_{1, n} \| f_{s, m}) &= \frac{1}{2} \left[\text{tr}(\Sigma_1^{-1} \Sigma_0) + (\mu_1 - \mu_0)^T \Sigma_1^{-1} (\mu_1 - \mu_0) \right. \\ &\quad \left. - k + \ln \left(\frac{\det(\Sigma_1)}{\det(\Sigma_0)} \right) \right]. \end{aligned} \quad (54)$$

Using the procedure above, we find the best fusion map and use it in the MB fusion (Section V-B2).

$$\prod_s f_s^d(\{\mathbf{y}_1, \dots, \mathbf{y}_n\} | \mathbf{Z}_s)^{\omega_s} \stackrel{(39)}{\approx} \prod_s \sum_{\sigma_s} \sum_{I_s \in \mathcal{F}_n(\mathbb{I}_s)} \prod_{i=1}^n r_{s, I_s(i)}^{\omega_s} f_{s, I_s(i)}(\mathbf{y}_{\sigma_s(i)})^{\omega_s} \prod_{k \in I_s^c(I_s)} (1 - r_{s,k})^{\omega_s} \quad (40)$$

$$= \sum_{\sigma_1} \sum_{I_1 \in \mathcal{F}_n(\mathbb{I}_1)} \prod_{i=1}^n r_{1, I_1(i)}^{\omega_1} f_{1, I_1(i)}(\mathbf{y}_{\sigma_1(i)})^{\omega_1} \prod_{k \in I_1^c(I_1)} (1 - r_{1,k})^{\omega_1} \quad (41)$$

$$\times \prod_{s>1} \sum_{\sigma_s} \sum_{I_s \in \mathcal{F}_n(\mathbb{I}_s)} \prod_{i=1}^n r_{s, I_s(i)}^{\omega_s} f_{s, I_s(i)}(\mathbf{y}_{\sigma_s(i)})^{\omega_s} \prod_{k' \in I_s^c(I_s)} (1 - r_{s,k'})^{\omega_s} \quad (41)$$

$$= \sum_{\sigma} \sum_{I_1 \in \mathcal{F}_n(\mathbb{I}_1)} \sum_{\theta \in \Theta_{I_1}} \prod_{i=1}^n r_{1, I_1(i)}^{\omega_1} f_{1, I_1(i)}(\mathbf{y}_{\sigma(i)})^{\omega_1} \quad (42)$$

$$\times \prod_{s>1} r_{s, [\theta(I_1(i))]_{s-1}}^{\omega_s} f_{s, [\theta(I_1(i))]_{s-1}}(\mathbf{y}_{\sigma(i)})^{\omega_s} \times \prod_{k \in I_1^c(I_1)} (1 - r_{1,k})^{\omega_1} \prod_{k' \in I_s^c(\theta(I_1))} (1 - r_{s,k'})^{\omega_s} \quad (42)$$

$$= \sum_{\sigma} \sum_{I_1 \in \mathcal{F}_n(\mathbb{I}_1)} \sum_{\theta \in \Theta_{I_1}} \tilde{w}_{I_1, \theta} \prod_{i=1}^n f_{\omega, I_1(i), \theta(I_1(i))}(\mathbf{y}_{\sigma(i)}) \quad (43)$$

VI. FILTER IMPLEMENTATION WITH GP-ET MODEL

Here, we first present the measurement and motion model for the spatial state of a single ET, where the target extent itself is described by a GP, extending the model from [5] to account for arbitrary sensor state (position, orientation). Prediction and update equations of an extended Kalman filter (EKF) filter using these models are given in the Appendix B. Finally, the prediction and update equations for the measurement rate and the predicted likelihood are stated, which is needed in the update step of the ET-PMB filter.

A. Description of ET Spatial State

We follow the approach of [5] to describe the single ET spatial state and its extent using a GP with input taking the angle expressed in the ET's local coordinate frame. The state thus comprises the ET center \mathbf{y}_c , the ET orientation ψ , and any additional quantities (e.g, velocity) in \mathbf{y}^* . The extent of the target is modeled as follows. Let u denote the local angle w.r.t. the ET orientation and y_i^f denotes the unknown target extent along input (angle) u_i , for a fixed and finite set of N angles. The target extent can thus be denoted by \mathbf{y}^f , which consists of points in the form

$$\mathbf{y}^f = [y^{f_1}, \dots, y^{f_N}]^T. \quad (55)$$

Then \mathbf{y}^f is modeled as a zero mean GP [42], [43]

$$\mathbf{y}^f \sim \mathcal{GP}(\mathbf{0}, K(\mathbf{u}, \mathbf{u})) \quad (56)$$

with covariance matrix

$$K(\mathbf{u}, \mathbf{u}) = \begin{bmatrix} k(u_1, u_1) & \dots & k(u_1, u_N) \\ k(u_N, u_1) & \dots & k(u_N, u_N) \end{bmatrix}. \quad (57)$$

Here, $k(\cdot, \cdot)$ is a periodic kernel function, the input of the GP is $\mathbf{u} = [u_1, \dots, u_N]^T$, and the output is \mathbf{y}^f .

Combining everything, the single ET spatial state including target extent is given by

$$\mathbf{y} = [(\bar{\mathbf{y}})^T, (\mathbf{y}^f)^T]^T, \quad (58)$$

where

$$\bar{\mathbf{y}} = [(\mathbf{y}_c)^T, \psi, \mathbf{y}^{*\top}]^T. \quad (59)$$

Remark 5: We utilize the kernel function proposed by [5]

$$k(u, u') = \sigma_f^2 \exp\left(-\frac{2 \sin^2\left(\frac{|u-u'|}{2}\right)}{l^2}\right) + \sigma_r^2, \quad (60)$$

where σ_f , l and σ_r are the (known) model hyper-parameters. Note that this function is 2π periodic, i.e., $k(u + 2\pi, u') = k(u, u')$, and, due to σ_r , star convex object shapes of different sizes can be described. See [5], [8] for further details and different choices for the kernel function to describe the extent of an ET with the help of a GP.

B. Measurement Model

A sensor s located at $\mathbf{p}_s \in \mathbb{R}^2$ with orientation α_s observes the ET contour in its local coordinate frame² resulting in measurement $\mathbf{z}^S \in \mathbb{R}^2$, where the following relationship holds

$$\mathbf{z}^S = h(\mathbf{y}) + \mathbf{w} \quad (61)$$

where $\mathbf{w} \sim \mathcal{N}(0, R)$ with measurement noise covariance R and

$$h(\mathbf{y}) = \mathbf{y}_c^S + \mathbf{e}(\theta^S)^T f(\theta^L), \quad (62)$$

where $\theta^S = \angle(\mathbf{z}^S - \mathbf{y}_c^S)$, $\mathbf{e}(\theta^S)$ is a unit vector in direction θ^S , and $\theta^L = \theta^S - \psi^S$ in which \mathbf{y}_c^S and ψ^S are the target location

²A quantity in the sensor coordinate frame is indicated by superscript S , in the ET coordinate frame by superscript L , and in the global coordinate frame by superscript G .

and orientation in the sensor frame of reference.³ Here, $f(\theta^L)$ is the extent of the target along local angle θ^L .

Due to the GP model, we follow [5] and express $f(\theta^L)$ as

$$f(\theta^L) = H^f(\theta^L)\mathbf{y}^f + e^f, \quad (63)$$

$$H^f(\theta^L) = K(\theta^L, \mathbf{u}^f)[K(\mathbf{u}^f, \mathbf{u}^f)]^{-1}, \quad (64)$$

in which $e^f \sim \mathcal{N}(0, k^f)$ with

$$k^f = k(\theta^L, \theta^L) - H^f(\theta^L)K(\theta^L, \mathbf{u}^f)^T. \quad (65)$$

Separating signal and noise contribution, and expressing the local states in global frame of reference through

$$\mathbf{y}_c^S = R(\alpha_s)(\mathbf{y}_c - \mathbf{p}_s) \quad (66)$$

$$\psi^S = \psi - \alpha_s, \quad (67)$$

where $R(\alpha)$ denotes the rotation matrix

$$R(\alpha) = \begin{bmatrix} \cos(\alpha) & -\sin(\alpha) \\ \sin(\alpha) & \cos(\alpha) \end{bmatrix}, \quad (68)$$

we find that with the GP contour model \mathbf{z}^S has a Gaussian distribution with mean

$$\tilde{h}(\mathbf{y}) = R(\alpha_s)(\mathbf{y}_c - \mathbf{p}_s) + e^T(\theta^S)H^f(\theta^L)\mathbf{y}^f \quad (69)$$

and covariance

$$\tilde{R} = R + k^f e(\theta^S) e^T(\theta^S). \quad (70)$$

1) *Motion Model*: The ET state moves according to the linear dynamic model

$$\bar{\mathbf{y}}_{k+1} = \bar{F}_k \bar{\mathbf{y}}_k + \bar{\mathbf{w}}_k, \quad (71)$$

where \bar{F}_k denotes the state transition matrix, and $\bar{\mathbf{w}}_k \sim \mathcal{N}(0, \bar{W}_k)$ with process noise covariance \bar{W}_k . The motion model of the ET contour is [5]

$$\mathbf{y}_{k+1}^f = F_k^f \mathbf{y}_k^f + \mathbf{w}_k^f, \quad (72)$$

where $F^f = e^{-\beta T} \mathbf{I}_N$ with \mathbf{I}_N the identity matrix of dimension N , and $\mathbf{w}_k^f \sim \mathcal{N}(0, W^f)$ with $W^f = (1 - e^{-2\beta T})K(\mathbf{u}^f, \mathbf{u}^f)$. Here, $\beta \geq 0$ denotes the forgetting factor allowing to accommodate targets with extents that change slowly, and T is the sampling time.

The measurement rate of the ET is assumed independent of the ETs' spatial state (c.f. (9)). This has been proposed in [30]. To allow the measurement rate to change over time an exponential forgetting factor $\frac{1}{\eta}$ is used in the motion model, where the predicted rate is [26], [30]

$$\alpha_{k|k-1} = \alpha_{k-1}/\eta, \quad (73)$$

$$\beta_{k|k-1} = \beta_{k-1}/\eta. \quad (74)$$

³Note that here the unknown angle θ^S is replaced by a point estimate, which is a simple but inaccurate approach and can be seen as a greedy association model [3]. It is also the approach taken by [5].

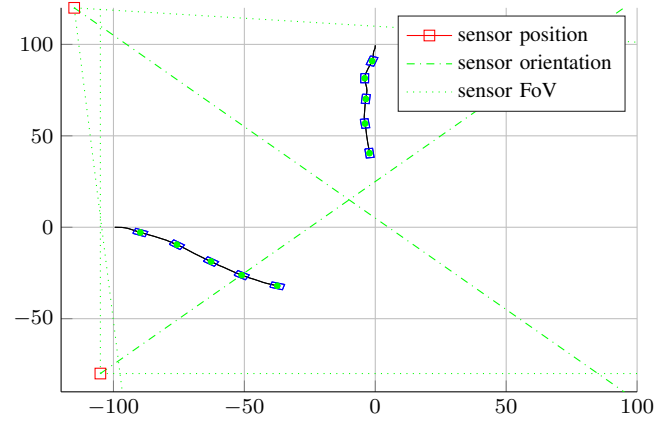


Fig. 1. Simulation scenario with two ETs observed by two sensors with overlapping FoVs. The ETs state is plot every 20 time steps.

2) *Independence Approximation*: Here, we follow [5], [44] to describe the recursive update of the GP model. With the help of Bayes law and the approximation that \mathbf{y}_k is a sufficient statistic for the measurements, the posterior on \mathbf{y}_k given all measurements $\mathbf{z}_{1:k}$ is

$$p(\mathbf{y}_k | \mathbf{z}_{1:k}) \propto p(\mathbf{z}_k | \mathbf{y}_k) p(\mathbf{y}_k | \mathbf{z}_{1:k-1}). \quad (75)$$

With the help of this independence approximation, the single ET spatial state can be predicted and updated over time leading to EKF prediction and update equations, which are derived in Appendix B. These are utilized in the prediction and update step of the ET-PMB filter (c.f. Section IV).

VII. NUMERICAL RESULTS

Here, we present simulation results using the independent ET-PMB filter with and without posterior fusion.

A. Setup

If not stated otherwise, there are two ETs present in the scene and their visibility and number of measurements produced per scan depends on the sensor FoV and its configuration. We use a rectangular target of length 5 m and width 3 m to model ETs representing vehicles. Furthermore, we use Lidar type sensors with the following simplified sensor models. Sensor 1 is located at $\mathbf{p}_{S_1} = [-115, 120]^T$, with orientation $\alpha_{S_1} = -45^\circ$, opening angle of 80° , angular resolution of 0.15° , and maximum range of 300 m. We generate a measurement when a ray from the sensor hits an ET and add noise with covariance matrix $R_{S_1} = 0.5\mathbf{I}_2$. Sensor 2 is located at $\mathbf{p}_{S_2} = [-105, -80]^T$, with orientation $\alpha_{S_2} = 45^\circ$, opening angle of 90° , angular resolution of 0.15° , maximum range of 300 m, and $R_{S_2} = 0.02\mathbf{I}_2$. Each sensor produces clutter measurements with rate $\lambda = 2$ and uniform spatial distribution $c(\mathbf{z}) = \mathcal{U}[-200, 200]^2$.

In the simulation, each independent ET-PMB filter has only access to measurements from one sensor (denoted indep. filter). The fusion filters are independent ET-PMB filters (denoted fusion filter), but perform posterior fusion according to Sec. V. If not stated otherwise, posterior fusion is

applied in every time step. Unless noted otherwise, we set $\omega_s = 1/N_{\text{sens}}$, resulting in a more conservative estimate than achievable. The fused posterior is then used as the prior for the next filter iteration. For comparison, an ET-PMB filter which incorporates measurements from all sensors is used (denoted centralized filter). There, measurements from each sensor are incorporated separately by applying multiple sequential ET-PMB filter update steps.

For all filter variants, spatially close measurements are clustered into measurement cells (c.f. Remark 2) using the DBSCAN clustering algorithm [45], where we set the maximum radius for the neighborhood to 4 m and the minimum number of points for a core point to 4. The simulation scenario is outlined in Fig. 1. The hyper parameters of the GP are $l^2 = \pi/8$, $\sigma_f^2 = 2$, $\sigma_r^2 = 2$, and 20 support points are used to track the target extent. Note that the dimension of the ET state is 26 (xy -position, orientation, xy -velocity, angular velocity, target extent support points). Target motion and the filter motion model are the same with sampling time $T = 0.5$ s,

$$\bar{F}_k = \begin{bmatrix} 1 & T \\ 0 & 1 \end{bmatrix} \otimes \mathbf{I}_3, \quad (76)$$

$$\bar{W}_k = \begin{bmatrix} \frac{T^3}{3} & \frac{T^2}{2} \\ \frac{T^2}{2} & T \end{bmatrix} \otimes \text{diag}([0.01, 0.01, 0.001]), \quad (77)$$

$\beta = 0.001$ in F_f (c.f. (72)), and the forgetting factor is set to $\frac{1}{\eta} = \frac{1}{1.11}$. In the filters, the birth intensity has rate $\lambda^b = \frac{1}{10}$ and for the spatial distribution we use a single Gaussian centered at location $x = [0, 100]^\top$ with covariance matrix $P = 30\mathbf{I}_2$. The probability of ET survival is $p_S = 0.999$, the probability of detection is $p_D = 0.99$.

B. Performance Metrics

Performance of estimated number of targets as well as their center location is assessed with the generalized optimal subpattern assignment (GOSPA) distance metric, which is defined as follows. Let sets $\hat{\mathbf{X}} = \{\mathbf{x}_1, \dots, \mathbf{x}_n\}$ and $\mathbf{Y} = \{\mathbf{y}_1, \dots, \mathbf{y}_m\}$ be finite subsets of \mathbb{R}^N , where without loss of generality $n \leq m$. Then [46], [47]

$$d_{\text{GOSPA}}^{(c, \alpha, p)} = \left(\min_{I_n \in \mathcal{F}_n(\{1, \dots, n\})} \sum_{i=1}^n d^{(c)}(\mathbf{x}_i, \mathbf{y}_{I_n(i)})^p + \frac{c^p}{\alpha} (m - n) \right)^{\frac{1}{p}}, \quad (78)$$

where we set the power parameter $p = 2$, cut-off distance $c = 20$, $\alpha = 2$, and $d^{(c)}(\mathbf{x}, \mathbf{y}) = \min(\|\mathbf{x} - \mathbf{y}\|_2, c)$, i.e., the minimum of the Euclidean distance and value c . To obtain $\hat{\mathbf{X}}$, we estimate the detected ETs from the (fused) posterior through comparison of the probability of existence of each Bernoulli component against the threshold $r_{\text{th}} = 0.5$ (c.f. Remark II-B). The set \mathbf{Y} contains the true ETs. Note that we only use the location of the target center.

Performance of the target extent estimation is assessed with the intersection over union (IOU) of the true target shape (in the global coordinate frame) and the estimated shape. Let A_k

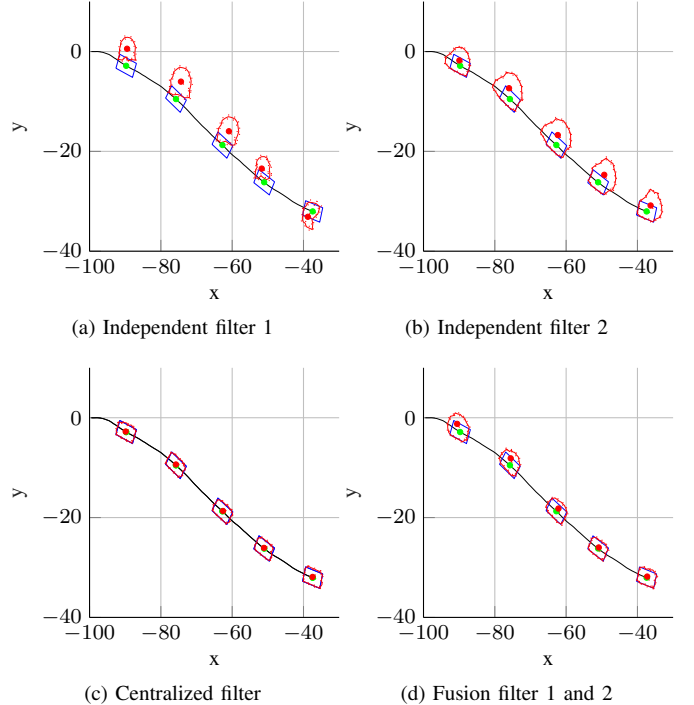


Fig. 2. Estimated shape of one ET for different ET-PMB filters. The true ET center and extent is plotted (green dot, blue solid line), as well as the estimated ones (red dot, red solid line for mean extent, red dotted line for one STD).

be the true ET area in xy -dimension at time step k , and \hat{A}_k its estimate. Then, the IOU is defined as, see, e.g., [5],

$$\text{IOU}(A_k, \hat{A}_k) = \frac{\text{area}(A_k \cap \hat{A}_k)}{\text{area}(A_k \cup \hat{A}_k)}. \quad (79)$$

Note that the IOU is, by definition, always between zero for non-overlapping target shapes and one when they fully overlap. Thus a well performing ETT filter will yield a high IOU for every ET. For both GOSPA and IOU average performance results were obtained by averaging over 50 Monte-Carlo runs.

C. Discussion of Results

Here, we first discuss the ETT filter performance with decentralized posterior fusion in terms of GOSPA and IOU performance metric. This is followed by performing posterior fusion at a lower rate. After that, we investigate the case when more than two ETT filters are used for posterior fusion, and finally we investigate the impact of the fusion weight w_i . We note that for well separated targets the simulation results using the summation over all possible fusion mappings for the MBs, as described in Section V-B2, and the summation only over the best fusion map, as presented in Section V-C, yield the same outcome. The benefit of using the latter is the reduced complexity. It is the method used in the simulations.

1) *Filter Performance with Posterior Fusion*: In Fig. 2, the true and estimated target state is plotted for ET 2 using the different filter variants. We observe that independent filter 1 (Fig. 2a) estimates the target state with a clear position error (in the positive y -direction). This filter uses measurements

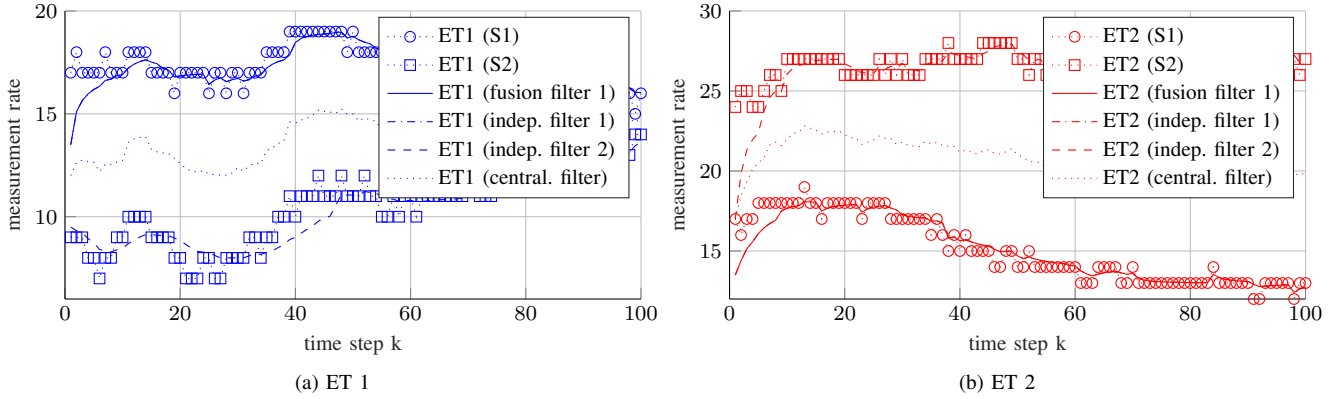


Fig. 3. The true and estimated measurement rate for each ET and sensor/filter is plotted over time.

from sensor 1, where most of the measurements provide information only from the ET's top edge due to the horizontal movement of the target and the sensor pose. In the measurement model (61), occlusions caused by the ET itself are not modeled. Due to the simple data association that is used, the received measurements can then be explained by an ET whose target contour is in proximity of the measurements and the target center is placed north of it. In contrast, independent filter 2 and the centralized filter estimate the target center closer to the true position (Fig. 2b and Fig. 2c). The former filter overestimates the target size in the direction where no measurement is provided, whereas the latter filter utilizes measurements from both sensors and can therefore estimate the target size accurately. The fusion filter utilizes information from both sensors through posterior fusion.

In Fig. 3, the true and estimated measurement rate γ is plotted over time. We can observe that the true measurement rate of the ETs is varying over time. Although only a simple process model for the measurement rate is used in the filters, they are able to correctly track the rate. This is true for all filter variants except the centralized filter. This filter performs two sequential filter update steps using measurement from different sensors. Since the number of measurements for an ET are different for each sensor, it follows that after centralized fusion the filter estimates the measurement rate of the ET incorrectly.

In Fig. 4, the average GOSPA is plotted over time for the simulation scenario illustrated in Fig. 1. The centralized filter has best performance followed by the fusion filter. Independent filter 2 has superior performance compared to the independent filter 1. Note that independent filter 1 is provided with measurements from sensor 1, which has a higher measurement noise compared to sensor 2.

In Table I, the average IOU is stated for the different ETs and filter variants. We observe that the IOU for ET 2 is low with independent filter 1 due to the misplaced target center, and with independent filter 2 due to the overestimation of the target size. The fusion and the centralized filter show comparable performance.

2) *Low Rate Posterior Fusion*: In a real system, it may not be feasible to perform posterior fusion after every filter update step. This can occur when the computers on which the filters

TABLE I
AVERAGE IOU

Filter	ET 1	ET 2
Independent 1	0.65	0.24
Independent 2	0.71	0.42
Fusion	0.72	0.76
Centralized	0.70	0.85

run are geographically separated and need to communicate over the wireless channel. Therefore, it is worthwhile to investigate the filter performance when posterior fusion is performed only every N time steps. In Fig. 5, the average GOSPA is plotted over time for fusion performed every $N = 15$ time steps. From the figure, we can observe that the fusion filters initially have the same performance as the independent filters because until $k = N$ no posterior fusion has been performed. At time step $k = 15$, posterior fusion is performed for the first time with the effect that the GOSPA value is reduced. Note that after the fusion step, the two fusion filters have the same posterior and therefore the same GOSPA value.

In Table II, the average GOSPA is stated for different values of N . We see that with increasing N the performance of the fusion filters deteriorates, since the information transfer (through fusion) between the filters over time is too low. Fusion filter 1 has worse performance compared to fusion filter 2 for $N \geq 15$, since it is equipped with the low quality sensor 1.

TABLE II
AVERAGE GOSPA

Filter	$N = 1$	$N = 15$	$N = 30$	$N = 50$
Fusion 1	1.08	1.61	2.20	2.83
Fusion 2	1.08	1.80	2.03	2.12
Independent 1	3.32	3.32	3.32	3.32
Independent 2	2.17	2.17	2.17	2.17
Centralized	0.89	0.89	0.89	0.89

3) *Posterior Fusion with more filters*: In Sec. V, we proposed a procedure to fuse PMB posteriors when there are more than two independent ET-PMB filters. We implement this sequentially, where first posteriors from two filters are fused.

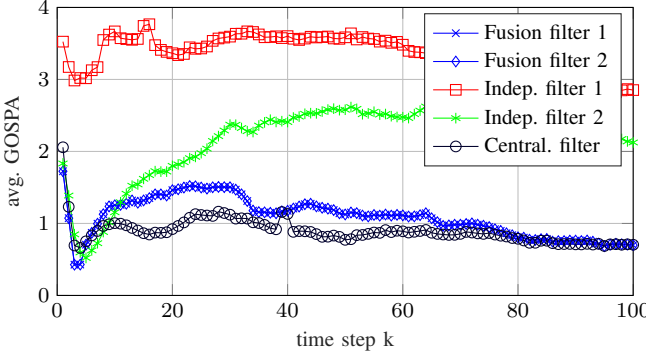


Fig. 4. The average GOSPA value is plotted over time. Posterior fusion is performed in every time step.

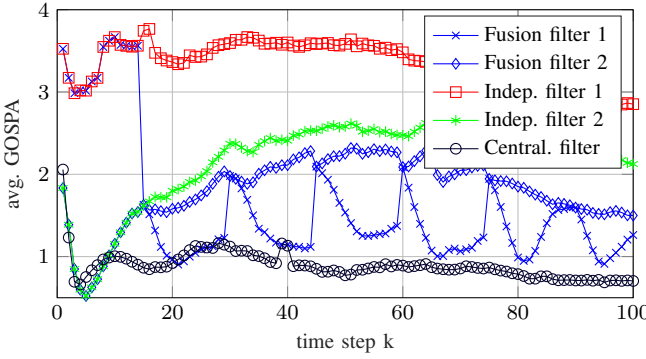


Fig. 5. The GOSPA value is plotted over time. Posterior fusion is performed only every $N = 15$ time steps.

The outcome is then used to fuse with a not yet fused posterior from one of the remaining filters. This process is repeated until all filter posteriors have been incorporated. We placed four sensors at $\mathbf{p}_{S_1} = [-150, -80]^\top$, $\mathbf{p}_{S_2} = [-150, -50]^\top$, $\mathbf{p}_{S_3} = [-150, -20]^\top$, and $\mathbf{p}_{S_4} = [-150, 10]^\top$ all with overlapping sensor FoVs towards the ETs. The remaining sensor parameters are the same as sensor 1 used in the previous simulations. In Table III, the average GOSPA, as well as the average IOU per ET are stated for a single independent ET-PMB filter (no fusion), two filters with posterior fusion performed after every filter update, and four filters with posterior fusion. With posterior fusion, performance increases, indicated by a decrease of the GOSPA value. Also the average IOU increases for all ETs with posterior fusion. Furthermore, fusion of two filter posteriors and four filter posteriors show similar performance in this scenario.

TABLE III
MULTIPLE POSTERIOR FUSION

No. Posteriors Fused	GOSPA	IOU (ET 1)	IOU (ET 2)
(no fusion)	1.22	0.61	0.62
2	0.89	0.66	0.67
4	0.86	0.68	0.66

4) *Impact of Fusion Weight Parameter:* The performance of the fusion filter for $\omega_s = 0.5$ for $s = \{1, 2\}$ as illustrated in Fig. 1 was stated in Table II. For $\omega_1 \simeq 1$ (and correspondingly $\omega_2 = 1 - \omega_1$), the fusion filter yields the same performance

as with independent filter 1. Likewise, for $\omega_1 \simeq 0$ the fusion filter has the same performance as with independent filter 2. Using the suboptimal adaptive method presented in Remark 3 executed prior to every posterior fusion step, resulted in an average GOSPA equal to using independent filter 2. The reason for this is that with constant process and measurement noise statistics independent of the ET's state, this approach selects the posterior which was updated by measurements with higher accuracy. Such an adaptive approach can be beneficial when, e.g., the sensor quality varies depending on the state of the ET.

VIII. CONCLUSIONS

We proposed a low-complexity decentralized PMB ETT filter that is capable of estimating the presence, state, and shape of ETs accurately with the help of a recently proposed GP model. The filter allows fusion of multiblobjetc densities from independent ETT filters for different sensors. Thereby, PPPs and MBs are separately fused in the minimum KLA sense yielding a fused posterior which is conservative but never overconfident about the estimated ETs. A low-complexity implementation is highlighted, relying on an assumption that the posterior of detected targets are spatially well separated, allowing the use of an optimal fusion map between pairs of sensors. The fusion map itself was identified by solving a linear optimal assignment problem based on a cost matrix comprised of the symmetric KLD between the detected target state estimates.

In the simulation results, we observed how the proposed independent ETT filter together with the GP model is capable of estimating the state and shape of the present ETs. Furthermore, we observed that robust fusion of the filters posterior allows to obtain a holistic view of the ETs in the sense that target state information from all filters is combined. This resulted in a reduced state estimation error quantified by the GOSPA distance metric and for the ET shape estimation by an increased area overlap quantified by the IOU metric.

We found that both the frequency of fusion and the fusion weights play an important role in the performance, deserving further study.

APPENDIX A ET-PMB PARAMETERS

Following [26, Sec. IV], we find that

$$w_A = \frac{\prod_{C \in A} \mathcal{L}_C}{\sum_{A \in \mathcal{A}} \prod_{C \in A} \mathcal{L}_C}, \quad (80)$$

$$\mathcal{L}_C = \begin{cases} \kappa^{C_C} + \langle D_+^u, \ell_{C_C} \rangle, & \text{if } C \cap \mathbb{I} = \emptyset, |C_C| = 1, \\ \langle D_+^u, \ell_{C_C} \rangle, & \text{if } C \cap \mathbb{I} = \emptyset, |C_C| > 1, \\ 1 - r_+^{i_C} + r_+^{i_C} \langle f_+^{i_C}, q_D \rangle, & \text{if } C \cap \mathbb{I} \neq \emptyset, C_C = \emptyset, \\ r_+^{i_C} \langle f_+^{i_C}, \ell_{C_C} \rangle, & \text{if } C \cap \mathbb{I} \neq \emptyset, C_C \neq \emptyset. \end{cases} \quad (81)$$

The density $f_C(\mathbf{X}^C)$ in (17) is a Bernoulli density with parameters

$$r_C = \begin{cases} \frac{\langle D_+^u, \ell_{C_C} \rangle}{\kappa_{C_C} + \langle D_+^u, \ell_{C_C} \rangle}, & \text{if } C \cap \mathbb{I} = \emptyset, |C_C| = 1, \\ 1, & \text{if } C \cap \mathbb{I} = \emptyset, |C_C| > 1, \\ \frac{r_+^{i_C} \langle f_+^{i_C}, q_D \rangle}{1 - r_+^{i_C} + r_+^{i_C} \langle f_+^{i_C}, q_D \rangle}, & \text{if } C \cap \mathbb{I} \neq \emptyset, C_C = \emptyset, \\ 1, & \text{if } C \cap \mathbb{I} \neq \emptyset, C_C \neq \emptyset, \end{cases} \quad (82)$$

$$f_C(\mathbf{x}) = \begin{cases} \frac{\ell_{C_C} D_+^u(\mathbf{x})}{\langle D_+^u, \ell_{C_C} \rangle}, & \text{if } C \cap \mathbb{I} = \emptyset, \\ \frac{q_D(\mathbf{x}) f_+^{i_C}(\mathbf{x})}{\langle f_+^{i_C}, q_D \rangle}, & \text{if } C \cap \mathbb{I} \neq \emptyset, C_C = \emptyset, \\ \frac{\ell_{C_C}(\mathbf{x}) f_+^{i_C}(\mathbf{x})}{\langle f_+^{i_C}, \ell_{C_C} \rangle}, & \text{if } C \cap \mathbb{I} \neq \emptyset, C_C \neq \emptyset. \end{cases} \quad (83)$$

APPENDIX B

ET PREDICTION AND UPDATE STEPS

Here, we first describe the EKF prediction and update steps for the ET's spatial state. This is followed by the update step of the ET measurement rate, and lastly the predicted likelihood utilized in the update step of the ET-PMB filter for the ET state model of Section VI.

A. ET spatial state

With the linear ET motion model the standard EKF prediction step with $\mathbf{y}_0 \sim \mathcal{N}(\hat{\mathbf{y}}_0, P_0)$ is [12]

$$\hat{\mathbf{y}}_{k|k-1} = F_k \hat{\mathbf{y}}_{k-1}, \quad (84)$$

$$P_{k|k-1} = F_k P_{k-1} F_k^\top + W_k, \quad (85)$$

where $F_k = \text{blkdiag}(\bar{F}_k, F_k^f)$, and $W_k = \text{blkdiag}(\bar{W}_k, W_k^f)$.

We now extend the EKF update steps derived in [5] to incorporate the (known) sensor state (position \mathbf{p}_s and orientation α_s). The standard EKF measurement update equations for a detection \mathbf{z}_k are [12]

$$H_k = \frac{d}{d\mathbf{y}_k} \tilde{h}(\mathbf{y})|_{\mathbf{y}=\hat{\mathbf{y}}_{k|k-1}}, \quad (86)$$

$$S_k = H_k P_{k|k-1} H_k^\top + R_k, \quad (87)$$

$$K_k = P_{k|k-1} H_k^\top S_k^{-1}, \quad (88)$$

$$\hat{\mathbf{y}}_k = \hat{\mathbf{y}}_{k|k-1} + K_k(\mathbf{z}_k - \tilde{h}(\hat{\mathbf{y}}_{k|k-1})), \quad (89)$$

$$P_k = P_{k|k-1} - K_k H_k P_{k|k-1}, \quad (90)$$

where $\tilde{h}(\cdot)$ was defined in (69) and (70). To linearize the measurement function, we need to compute [5]

$$H_k = \left[\frac{d\tilde{h}(\mathbf{y})}{d\mathbf{y}_c}, \frac{d\tilde{h}(\mathbf{y})}{d\psi}, \frac{d\tilde{h}(\mathbf{y})}{d\mathbf{y}^*}, \frac{d\tilde{h}(\mathbf{y})}{d\mathbf{y}^f} \right], \quad (91)$$

where in our case $\frac{d\tilde{h}(\mathbf{y})}{d\mathbf{y}^*} = 0$. We further get

$$\frac{d\tilde{h}(\mathbf{y})}{d\mathbf{y}^f} = e(\theta^S) H^f(\theta^L), \quad (92)$$

$$\frac{d\tilde{h}(\mathbf{y})}{d\psi} = e(\theta^S) \frac{d}{d\psi} H^f(\theta^L) \mathbf{y}^f, \quad (93)$$

$$\frac{d}{d\psi} H^f(\theta^L) = - \frac{\partial}{\partial u} H^f(u) \Big|_{u=\theta^L}, \quad (94)$$

where [5]

$$\frac{dH^f(u)}{du} = \frac{d}{du} K(u, \mathbf{u}^f) [K(\mathbf{u}^f, \mathbf{u}^f)]^{-1}, \quad (95)$$

$$\frac{dK(u, \mathbf{u}^f)}{du} = \frac{d}{du} [k(u, u_1^f), \dots, k(u, u_N^f)], \quad (96)$$

$$\frac{dk(u, u_i^f)}{du} = - \frac{1}{l^2} \sin(u - u_i^f) k(u, u_i^f). \quad (97)$$

Further,

$$\begin{aligned} \frac{d\tilde{h}(\mathbf{y})}{d\mathbf{y}_c} &= R(\alpha_s) + \frac{d}{d\mathbf{u}} e(\mathbf{u}) \Big|_{\mathbf{u}=\mathbf{y}_c} (H^f(\theta^L) \mathbf{y}^f)^\top + e(\mathbf{y}_c) \\ &\times \left(\left(\left(\frac{d}{du} H^f(u) \Big|_{u=\theta^L} \right)^\top \frac{d}{d\mathbf{w}} \theta^L(\mathbf{w}) \Big|_{\mathbf{w}=\mathbf{y}_c} \right)^\top \mathbf{y}^f \right)^\top, \end{aligned} \quad (98)$$

where [5]

$$\frac{d}{d\mathbf{u}} e(\mathbf{u}) = \frac{(\mathbf{z}^S - \mathbf{u})(\mathbf{z}^S - \mathbf{u})^\top}{\|\mathbf{z}^S - \mathbf{u}\|^3} - \frac{1}{\|\mathbf{z}^S - \mathbf{u}\|} \mathbf{I}_2, \quad (99)$$

$$\begin{aligned} \frac{d}{d\mathbf{w}} \theta^L(\mathbf{w}) &= \frac{1}{\|\mathbf{z}^S - \mathbf{y}_c^S\|^2} \\ &\times \left[\mathbf{z}^{S^Y} - \mathbf{y}_c^{S^Y}, -(\mathbf{z}^{S^X} - \mathbf{y}_c^{S^X}) \right] R(\alpha_s). \end{aligned} \quad (100)$$

Here, the superscript \mathbf{b}^X and \mathbf{b}^Y correspond to the first and second dimension of the vector \mathbf{b} . Furthermore, we wrote $e(\mathbf{y}_c)$ for $e(\theta^S)$ to indicate the state dependency.

To update the ET spatial state by a set of detections $\mathbf{W} = \{\mathbf{z}_{k,l}\}_{l=1}^{n_k}$, we augment the measurement vector

$$\mathbf{z}_k = [\mathbf{z}_{k,1}^\top, \dots, \mathbf{z}_{k,n_k}^\top]^\top, \quad (101)$$

where

$$R_k = \text{diag}(R_{k,1}, \dots, R_{k,n_k}), \quad (102)$$

$$\tilde{h}_k(\mathbf{y}_k) = [\tilde{h}_{k,1}(\mathbf{y}_k)^\top, \dots, \tilde{h}_{k,n_k}(\mathbf{y}_k)^\top]^\top. \quad (103)$$

B. ET measurement rate

The predicted ET's measurement rate $\gamma_{k|k-1}$ has parameters $\alpha_{k|k-1}$ and $\beta_{k|k-1}$ (c.f. (9), (74)), which are updated for a set of detections \mathbf{W} by [26]

$$\alpha_k = \alpha_{k|k-1} + |\mathbf{W}|, \quad (104)$$

$$\beta_k = \beta_{k|k-1} + 1. \quad (105)$$

C. Predicted likelihood for ET-PMB filter

The predicted likelihood, used in the update step of the ET-PMB filter (c.f. Sec. IV-C), for a set of detections \mathbf{W} for a single ET is

$$\ell_{\mathbf{W}} = \frac{\Gamma(\alpha_k) \beta_{k|k-1}^{\alpha_{k|k-1}}}{\Gamma(\alpha_{k|k-1}) \beta_k^{\alpha_k}} \prod_{l=1}^{|\mathbf{W}|} \mathcal{N}(\mathbf{z}_{k,l} - \tilde{h}(\hat{\mathbf{y}}_{k|k-1,l}), S_{k,l}). \quad (106)$$

REFERENCES

[1] Y. Bar-Shalom and X.-R. Li, *Multitarget-multisensor tracking: principles and techniques*. YBs London, UK; 1995, vol. 19.

[2] R. P. S. Mahler, *Statistical multisource-multitarget information fusion*. Artech House, Inc., 2007.

[3] K. Granström, M. Baum, and S. Reuter, "Extended Object Tracking: Introduction, Overview, and Applications," *JAIF Journal of Advances in Information Fusion*, vol. 12, no. 2, pp. 139–174, Dec. 2017.

[4] J. W. Koch, "Bayesian approach to extended object and cluster tracking using random matrices," *IEEE Transactions on Aerospace and Electronic Systems*, vol. 44, no. 3, pp. 1042–1059, 2008.

[5] N. Wahlström and E. Özkan, "Extended target tracking using Gaussian processes," *IEEE Transactions on Signal Processing*, vol. 63, no. 16, pp. 4165–4178, 2015.

[6] E. Özkan, N. Wahlström, and S. J. Godsill, "Rao-Blackwellised particle filter for star-convex extended target tracking models," in *19th International Conference on Information Fusion (FUSION)*. IEEE, 2016, pp. 1193–1199.

[7] W. Aftab, A. De Freitas, M. Arvaneh, and L. Mihaylova, "A Gaussian process approach for extended object tracking with random shapes and for dealing with intractable likelihoods," in *2017 22nd International Conference on Digital Signal Processing (DSP)*. IEEE, 2017, pp. 1–5.

[8] T. Hirscher, A. Scheel, S. Reuter, and K. Dietmayer, "Multiple extended object tracking using Gaussian processes," in *2016 19th International Conference on Information Fusion (FUSION)*. IEEE, 2016, pp. 868–875.

[9] A. Scheel, S. Reuter, and K. Dietmayer, "Using separable likelihoods for laser-based vehicle tracking with a labeled multi-Bernoulli filter," in *2016 19th International Conference on Information Fusion (FUSION)*. IEEE, 2016, pp. 1200–1207.

[10] ———, "Vehicle tracking using extended object methods: An approach for fusing radar and laser," in *2017 IEEE International Conference on Robotics and Automation (ICRA)*. IEEE, 2017, pp. 231–238.

[11] M. Michaelis, P. Berthold, D. Meissner, and H.-J. Wuensche, "Heterogeneous multi-sensor fusion for extended objects in automotive scenarios using Gaussian processes and a GMPHD-filter," in *Sensor Data Fusion: Trends, Solutions, Applications (SDF)*, 2017. IEEE, 2017, pp. 1–6.

[12] D. Simon, *Optimal state estimation: Kalman, H infinity, and nonlinear approaches*. John Wiley & Sons, 2006.

[13] J. K. Uhlmann, "General data fusion for estimates with unknown cross covariances," in *Signal Processing, Sensor Fusion, and Target Recognition V*, vol. 2755. International Society for Optics and Photonics, 1996, pp. 536–548.

[14] R. P. S. Mahler, "Optimal/robust distributed data fusion: a unified approach," in *Signal Processing, Sensor Fusion, and Target Recognition IX*, vol. 4052. International Society for Optics and Photonics, 2000, pp. 128–139.

[15] D. Clark, S. Julier, R. Mahler, and B. Ristic, "Robust multi-object sensor fusion with unknown correlations," in *Sensor Signal Processing for Defence (SSPD)*. IET, 2010.

[16] M. B. Guldogan, "Consensus Bernoulli Filter for Distributed Detection and Tracking using Multi-Static Doppler Shifts," *IEEE Signal Processing Letters*, vol. 21, no. 6, pp. 672–676, 2014.

[17] M. Üney, S. Julier, D. Clark, and B. Ristic, "Monte Carlo realisation of a distributed multi-object fusion algorithm," in *Sensor Signal Processing for Defence (SSPD)*. IET, 2010.

[18] M. Üney, D. E. Clark, and S. J. Julier, "Distributed fusion of PHD filters via exponential mixture densities," *IEEE Journal of Selected Topics in Signal Processing*, vol. 7, no. 3, pp. 521–531, 2013.

[19] T. Li, J. M. Corchado, and S. Sun, "On generalized covariance intersection for distributed PHD filtering and a simple but better alternative," in *20th International Conference on Information Fusion (Fusion)*. IEEE, 2017, pp. 1–8.

[20] G. Battistelli, L. Chisci, C. Fantacci, A. Farina, and A. Graziano, "Consensus CPHD filter for distributed multitarget tracking," *IEEE Journal of Selected Topics in Signal Processing*, vol. 7, no. 3, pp. 508–520, 2013.

[21] G. Battistelli, L. Chisci, C. Fantacci, A. Farina, and B.-N. Vo, "Average Kullback-Leibler divergence for random finite sets," in *18th International Conference on Information Fusion (Fusion)*. IEEE, 2015, pp. 1359–1366.

[22] C. Fantacci, B.-N. Vo, B.-T. Vo, G. Battistelli, and L. Chisci, "Consensus labeled random finite set filtering for distributed multi-object tracking," *arXiv preprint arXiv:1501.01579*, 2015.

[23] B. Wang, W. Yi, R. Hoseinnezhad, S. Li, L. Kong, and X. Yang, "Distributed fusion with multi-Bernoulli filter based on generalized covariance intersection," *IEEE Transactions on Signal Processing*, vol. 65, no. 1, pp. 242–255, 2017.

[24] S. Li, W. Yi, R. Hoseinnezhad, G. Battistelli, B. Wang, and L. Kong, "Robust distributed fusion with labeled random finite sets," *IEEE Transactions on Signal Processing*, vol. 66, no. 2, pp. 278–293, 2017.

[25] J. L. Williams, "Marginal multi-bernoulli filters: RFS derivation of MHT, JIPDA, and association-based MemBer," *IEEE Transactions on Aerospace and Electronic Systems*, vol. 51, no. 3, pp. 1664–1687, Jul. 2015.

[26] K. Granström, M. Fatemi, and L. Svensson, "Poisson multi-Bernoulli conjugate prior for multiple extended object estimation," *arXiv preprint arXiv:1605.06311*, 2016.

[27] K. Granström, M. Fatemi, and L. Svensson, "Gamma Gaussian inverse-Wishart Poisson multi-Bernoulli filter for extended target tracking," in *19th International Conference on Information Fusion (FUSION)*. IEEE, 2016, pp. 893–900.

[28] R. P. S. Mahler, *Advances in Statistical Multisource-Multitarget Information Fusion*. Artech House, 2014.

[29] A. F. García-Fernández, J. Williams, K. Granström, and L. Svensson, "Poisson multi-Bernoulli mixture filter: direct derivation and implementation," *IEEE Transactions on Aerospace and Electronic Systems*, vol. 54, no. 4, Aug. 2018.

[30] K. Granström and U. Orguner, "Estimation and maintenance of measurement rates for multiple extended target tracking," in *2012 15th International Conference on Information Fusion (FUSION)*. IEEE, 2012, pp. 2170–2176.

[31] K. Granström, C. Lundquist, and O. Orguner, "Extended target tracking using a Gaussian-mixture PHD filter," *IEEE Transactions on Aerospace and Electronic Systems*, vol. 48, no. 4, pp. 3268–3286, 2012.

[32] K. Granström and U. Orguner, "A PHD filter for tracking multiple extended targets using random matrices," *IEEE Transactions on Signal Processing*, vol. 60, no. 11, pp. 5657–5671, Nov. 2012.

[33] C. Lundquist, K. Granström, and U. Orguner, "An extended target CPHD filter and a gamma Gaussian inverse Wishart implementation," *IEEE Journal of Selected Topics in Signal Processing, Special Issue on Multi-target Tracking*, vol. 7, no. 3, pp. 472–483, Jun. 2013.

[34] J. L. Williams, "An efficient, variational approximation of the best fitting multi-Bernoulli filter," *IEEE Transactions on Signal Processing*, vol. 63, no. 1, pp. 258–273, 2015.

[35] Y. Xia, K. Granström, L. Svensson, and M. Fatemi, "Extended Target Poisson Multi-Bernoulli Filter," *arXiv preprint arXiv:1801.01353*, 2018.

[36] J. L. Williams, "Graphical model approximations of random finite set filters," *arXiv preprint arXiv:1105.3298*, 2011.

[37] P. Bromiley, "Products and convolutions of Gaussian probability density functions," *Tina-Vision Memo*, vol. 3, no. 4, p. 1, 2003.

[38] B.-T. Vo and B.-N. Vo, "Labeled random finite sets and multi-object conjugate priors," *IEEE Transactions on Signal Processing*, vol. 61, no. 13, pp. 3460–3475, 2013.

[39] Y. Bar-Shalom, "Multitarget-multisensor tracking: advanced applications," *Artech House, Norwood, MA*, 1990.

[40] J. Munkres, "Algorithms for the assignment and transportation problems," *Journal of the society for industrial and applied mathematics*, vol. 5, no. 1, pp. 32–38, 1957.

[41] F. Bourgeois and J.-C. Lassalle, "An extension of the Munkres algorithm for the assignment problem to rectangular matrices," *Communications of the ACM*, vol. 14, no. 12, pp. 802–804, 1971.

[42] C. E. Rasmussen and C. K. I. Williams, *Gaussian processes for machine learning*. MIT Press, 2006.

[43] C. M. Bishop, *Pattern Recognition and Machine Learning*. Springer, 2006.

[44] M. F. Huber, "Recursive Gaussian process: On-line regression and learning," *Pattern Recognition Letters*, vol. 45, pp. 85–91, 2014.

[45] M. Ester, H.-P. Kriegel, J. Sander, X. Xu *et al.*, "A density-based algorithm for discovering clusters in large spatial databases with noise," in *Kdd*, vol. 96, no. 34, 1996, pp. 226–231.

[46] A. S. Rahmathullah, Á. F. García-Fernández, and L. Svensson, "A metric on the space of finite sets of trajectories for evaluation of multi-target tracking algorithms," *arXiv preprint arXiv:1605.01177*, 2016.

[47] ———, "Generalized optimal sub-pattern assignment metric," in *2017 20th International Conference on Information Fusion (Fusion)*. IEEE, 2017, pp. 1–8.



Markus Fröhle (S'11) received the B.Sc. and M.Sc. degrees in Telematics from Graz University of Technology, Graz, Austria, in 2009 and 2012, respectively. From 2012 to 2013, he was a Research Assistant with the Signal Processing and Speech Communication Laboratory, Graz University of Technology. Since 2013 he is working towards the Ph.D. degree in electrical engineering with the Department of Electrical Engineering, Chalmers University of Technology, Gothenburg, Sweden. His current research interests include signal processing for wireless multi-agent systems, and localization and tracking.



Karl Granström (M'08) is a postdoctoral research fellow at the Department of Signals and Systems, Chalmers University of Technology, Gothenburg, Sweden. He received the MSc degree in Applied Physics and Electrical Engineering in May 2008, and the PhD degree in Automatic Control in November 2012, both from Linköping University, Sweden. He previously held postdoctoral positions at the Department of Electrical and Computer Engineering at University of Connecticut, USA, from September 2014 to August 2015, and at the Department of Electrical Engineering of Linköping University from December 2012 to August 2014. His research interests include estimation theory, multiple model estimation, sensor fusion and target tracking, especially for extended targets. He received paper awards at the Fusion 2011 and Fusion 2012 conferences. He has organised several workshops and tutorials on the topic Multiple Extended Target Tracking and Sensor Fusion.



Henk Wymeersch (S'01, M'05) obtained the Ph.D. degree in Electrical Engineering/Applied Sciences in 2005 from Ghent University, Belgium. He is currently a Professor of Communication Systems with the Department of Electrical Engineering at Chalmers University of Technology, Sweden. Prior to joining Chalmers, he was a postdoctoral researcher from 2005 until 2009 with the Laboratory for Information and Decision Systems at the Massachusetts Institute of Technology. Prof. Wymeersch served as Associate Editor for IEEE Communication Letters (2009-2013), IEEE Transactions on Wireless Communications (since 2013), and IEEE Transactions on Communications (2016-2018). His current research interests include cooperative systems and intelligent transportation.